Polyoxomolybdate based Ionic-Liquids as Active Catalysts for Oxidative Desulfurization of Simulated Diesel

Fatima Mirante,[a] Neide Gomes,[b] Marta Corvo,[c] Sandra Gago,[b*] and Salete S. Balula,[a*]

[a] *LAQV-REQUIMTE, Departamento de Química e Bioquímica, Faculdade de Ciências, Universidade do Porto, 4169-007 Porto, Portugal*

[b] *LAQV-REQUIMTE, Departamento de Química, Faculdade de Ciências e Tecnologia, Universidade NOVA de Lisboa, 2829-516 Monte da Caparica, Portugal*

[b] *CENIMAT/I3N, Faculdade de Ciências e Tecnologia, Universidade Nova de Lisboa, 2829-516 Monte da Caparica, and AD Física, ISEL/IPL, R. Conselheiro Emídio Navarro, 1, 1959-007 Lisboa, Portugal*

***In memorial**:*

This publication is dedicated in memorial of Professor Doctor Ana Cavaleiro, an enthusiastic professor with a "scientific passion" for Polyoxometalates: structures and applications.

Abstract

This work compares the stability and the catalytic efficiency of different ionic liquid phosphomolybdates ($[BPy]_3[PMo_{12}O_{40}]$ and $[BMIM]_3[PMo_{12}O_{40}]$) with a cationic (propylpyridinium) functionalized mesoporous silica nanoparticle composite ($PMo_{12}O_{40}$@PPy-MSN). These were used as solid catalysts for the oxidative desulfurization of a multicomponent model diesel using hydrogen peroxide as oxidant and a polar immiscible extraction solvent. Ionic liquid ($[BMIM][PF_6]$ was successfully used as solvent to extract sulfur compounds from model diesel. The ionic liquid phosphomolybdates showed partial solubility in the ionic liquid phase, occurring some decomposition of their Keggin structure in the soluble reaction media, probably caused by their interaction with oxidant. On the other hand, the phosphomolybdate composite $PMo_{12}O_{40}$@PPy-MSN presented high structural stability and only negligible leaching occurrence after various consecutive reaction cycles. The model diesel was near complete desulfurized after

3 h and consecutive desulfurization cycles were performed without loss of activity. Therefore, the immobilization of Keggin phosphomolybdate structure $[PMo_{12}O_{40}]^{3-}$ using cationic propylpyridinium silica nanoparticle is an assertive strategy to produce stable and active heterogeneous catalysts.

KEYWORDS: Mesoporous Silica Nanoparticles; Polyoxomolybdate; Heterogeneous Catalysis; Oxidative Desulfurization; Fuels

Introduction

One of serious environmental problem is the harmful emission of SOx during combustion of fuels.[1, 2] In order to reduce the emissions of these compounds to the atmosphere, strict regulations have been implemented worldwide limiting the sulfur level in fuels (S-content < 10 ppm). Actually, petroleum industry use the hydrotreating method (HDS) to remove an important series of sulfur compounds (thiols, sulfides and disulfides) from fuel.[3] However, the most refractory sulfur compounds (mostly benzothiophene derivatives) in fuels are still very hard or costly to remove.[4, 5] One of the most promising alternative to the HDS techniques is the extractive and catalytic oxidative desulfurization (ECODS) method.[6-8] The ECODS process allows for the sustainable deep desulfurization of fuels by operating under mild conditions, using green oxidants, extracting agents, such as ionic liquid, acetonitrile and methanol.[8-13]

Our research group has been designing novel and highly efficient desulfurization systems based on polyoxometalates (POMs) for application in model and real diesels under sustainable conditions.[5, 14-20] POMs are exceptional candidates for catalytic applications due to redox properties, chemical robustness and thermal stability. [21] To prepare stable heterogeneous catalysts it is convenient to immobilize the POMs in solid supports that allow their recovery and reuse. Silica-based materials are among the most used supports for heterogenization of active catalytic species, including POMs.[22]. Mesoporous silica nanoparticles (MSNs) possess ordered porosity, high surface area-to-volume ratio, controllable pore size and can be easily functionalized. [23, 24] These properties may even improve the performance of materials in terms of energy and power density, lifetime and stability, make them ideal for use as supports for adsorption, catalysis, chemical separations and fuel cells.[25-33] Although silica mesoporous materials have been

widely explored as catalytic supports as well as adsorbents for desulfurization studies, the application of the corresponding nanoparticles is still relatively scarce.[34]

In this work, two ionic liquids $[BPy]_3[PMo_{12}O_{40}]$ and $[BMIM]_3[PMo_{12}O_{40}]$, were prepared based on the Keggin structure $[PMo_{12}O_{40}]^{3-}$ anion and 1-butylpyridinium and 1-butyl-3-methylimidazolium as organic cations, respectively. Their structures were confirmed by solution ^{1}H and ^{31}P NMR, FTIR spectroscopies and by elemental analysis. The composite material $PMo_{12}O_{40}$@PPy-MSN was also prepared by immobilization of the Keggin $[PMo_{12}O_{40}]^{3-}$ anion on MSNs functionalized with the propylpyridinium cation. This material was characterized by elemental and ICP-OES analyses, SEM/EDS, TEM, FTIR , solid state ^{31}P and ^{13}C NMR and FTIR spectroscopies . All catalysts were tested in extractive catalytic oxidative desulfurization ECODS processes, using a multicomponent model diesel, under sustainable conditions (reduced toxicity, using hydrogen peroxide oxidant and ionic liquid solvent).

2. Experimental

2.1. Materials and methods

All the reagents used in the POM and materials syntheses, namely phosphomolybdic acid hydrate (Aldrich), tetrabutylammonium bromide ($(C_{16}H_{36}N)Br$, Aldrich), polyoxyethylene cetyl ether (Brij-56, Aldrich), tetraethyl orthosilicate 98% (TEOS, Aldrich), ethyl acetate (Aldrich), n-cetyltrimethylammonium bromide (CTAB, BDH Chemicals), pluronic F127 (Aldrich), triethanolamine (TEA, Alfa Aesar), 1-chlorobutane (Alfa Aesar, >99%); 3-iodopropyltrimethoxysilane (Sigma-Aldrich, >95%), 1-butyl-3-methylimidazolium chloride, [BMIM]Cl (Solchemar, >99%); pluronic F127 (Sigma-Aldrich), pyridine (Merck, p.a.); tetraethylorthosilicate (TEOS) (Sigma-Aldrich, 98%), triethanolamine (TEA) (Alfa Aesar, >98%); n-cetyltrimethylammonium bromide, CTAB (BDH Chemicals, >99%), Amberlyst A-26 (OH) (Alfa Aesar), were used as received. The reagents for ODS studies, including 1-benzothiophene (1-BT, Fluka), dibenzothiophene (DBT, Aldrich), 4-methyldibenzothiophene (4-MDBT, Aldrich), 4,6-dimethyldibenzothiophene (4,6-DMDBT, Alfa Aesar), *n*-octane (Aldrich), acetonitrile (MeCN, Fisher Chemical), 1-butyl-3-methylimidazolium hexafluorophosphate ($[BMIM][PF_6]$, Sigma-Aldrich) and H_2O_2 30% w/v (Aldrich) were purchased from chemical suppliers and used

without further purification. FT-IR spectra were recorded in the 400–4000 cm^{-1} region on a Bruker Tensor 27 Spectrometer using KBr pellets for solid samples and NaCl cells for oily samples. Solution ^{1}H and ^{31}P NMR spectra were recorded at 400.13 MHz and 162 MHz, respectively, with a Bruker AMX400 and a Bruker Avance III 400 spectrometer and chemical shifts are given with respect to external 85% H_3PO_4. Solid state ^{13}C and ^{31}P MAS NMR spectra were acquired with a 7 T (300 MHz) AVANCE III Bruker spectrometer operating respectively at 75 MHz (^{13}C) and 121 MHz (^{31}P), equipped with a BBO probe head. The samples were spun at the magic angle at a frequency of 5 kHz in 4 mm-diameter rotors at room temperature. The ^{13}C MAS NMR experiments were acquired with proton cross polarization (CP MAS) with a contact time of 1.2 ms, and the recycle delay was 2.0 s. The ^{31}P MAS NMR spectra were obtained by a single pulse sequence with a 90° pulse of 10.5 μs at a power of 20 W, and a relaxation delay of 82.0 s. Elemental analyses (CHN) were performed using a Thermofinnigan Flash EA 112 series (LAQV-FCT) and Mo by ICP-OES on a Perkin Elmer Optima 4300 DV instrument (University of Santiago de Compostela). Transmission electron microscopy (TEM) images were obtained using a Hitachi H-8100 microscope with thermionic emission (LaB6) and 200 kV acceleration voltage at MicroLAb (Instituto Superior Técnico). The samples were supported on carbon-coated copper grids and the digital image acquisition was performed with a CCD MegaView II bottom-mounted camera. Scanning electron microscopy (SEM) and energy dispersive X-ray spectroscopy (EDS) studies were performed at the "Centro de Materiais da Universidade do Porto" (CEMUP, Porto, Portugal) using a JEOL JSM 6301F scanning electron microscope operating at 15 kV equipped with an Oxford INCA Energy 350 energy-dispersive X-ray spectrometer. The samples were studied as powders and were previously subjected to gold sputtering. GC-FID was carried out in a Varian CP-3380 chromatograph to monitor the ODS multicomponent model oil experiments. Hydrogen was used as the carrier gas (55 cm s^{-1}) and fused silica Supelco capillary columns SPB-5 (30 m x 0.25 mm i.d.; 25 μm film thickness) were used.

2.2. Synthesis of 1-butylpyridinium chloride [BPy] [Cl]

This synthesis was performed in 1.4:1 molar ratio, by heating 1-chlorobutane (9.3 mL, 88.5 mmol) and pyridine (5.1 mL, 63.2 mmol) without solvent at 100 °C for 48 h. The final product was washed with diethyl ether (3x20 mL) and dried under vacuum. The final product was obtained as a brownish solid (3.69 g, 28 %).

^{1}H NMR (400.13 MHz, $CDCl_3$, r.t) δ = 9.70 (d, J = 4.0 Hz, 2H), 8.50 (t, J = 4.0 Hz, 1H), 8.16 (t, J = 8.0 Hz, 2H), 5.02 (t, J = 8.0 Hz, 2H), 2.05 (m, 2H), 1.40 (m, 2H), 0.93 (t, J = 8.0 Hz, 3H) ppm. **Selected FTIR** (cm^{-1}, NaCl cell): 3417 (m); 3079 (m); 3025 (m); 3000 (m); 2961 (m); 2934 (m); 2874 (m); 2361 (m); 1986 (m); 1920 (m); 1868 (m); 1580 (s); 1482 (m); 1438 (s); 1380 (m); 1313 (m); 1287 (m); 1242 (m); 1216 (m); 1146 (m); 1068 (m); 1030 (m); 991 (m); 931 (m); 873 (m); 747 (m); 704 (m); 649 (m); 602 (m).

2.3. Synthesis of $[BPy]_3[PMo_{12}O_{40}]$

1-butylpyridinium chloride [BPy][Cl] (0.2580 g, 1.46 mmol) was dissolved in 15 mL of methanol and to this solution the ion exchange resin Amberlyst® A26 (OH-) (9.13 mL, 7.3 mmol) was added and it was kept in stirring for 1h in order to exchange the chloride to the hydroxide form. The resin was filtered and washed with methanol. To the resultant filtrate, $H_3PMo_{12}O_{40}$ (0.973 g, 0.53 mmol) in methanol was slowly added, a yellow precipitate immediately formed and the mixture was stirred at room temperature for 1 h. The product was filtered, washed several times with methanol and dried in the oven at 80 °C overnight (1.05 g, 89 %).

^{1}H NMR (400.13 MHz, DMSO d6, 25 ºC) δ = 9.10 (d, J = 4.0 Hz, 2 H), 8.63 (t, J = 8.0 Hz, 1H), 8.19 (t, J = 8.0 Hz 2H), 4.63 (t, J = 8.0 Hz, 2H), 1.95 (m, J = 8.0 Hz, 2H), 1.31 (m, 2H), 0.94 (t, J = 8.0 Hz, 3H) ppm. **^{31}P NMR** (162 MHz, CD_3CN, 25 ºC) δ = -2.09 ppm. **Selected FTIR** (cm^{-1}, KBr): 3124 (w), 3080 (w), 3063 (w), 2963 (w), 2929 (w), 2869 (w), 1632 (s), 1581 (w), 1485 (s), 1462 (m), 1384 (w), 1316 (w), 1278 (w), 1209 (w), 1168 (m), 1063 (vs), 956 (vs), 878 (s), 795 (s), 682 (s), 644 (w), 594 (w), 504 (m). Anal. calcd. for $(C_9H_{14}N)_3PMo_{12}O_{40}$ (2230.87): C, 15.04; H, 1.88; N, 1.87; Found: C, 14.76; H, 1.85; N, 1.87

2.4. Synthesis of $[BMIM]_3[PMo_{12}O_{40}]$ catalyst

This catalyst was prepared using the same method described above. 1-Butyl-3-methylimidazolium chloride, [BMIM][Cl], (0.231 g, 1.3 mmol) was dissolved in 15 mL of methanol and to this solution the ion exchange resin Amberlyst® A26 (OH-) (8.4 mL, 6.7 mmol) was added. The mixture was stirred for 1h at room temperature and the resin was filtered and washed with methanol. To the resultant filtrate, $H_3PMo_{12}O_{40}$ (0.905 g, 0.43 mmol) in methanol was slowly added, a yellow precipitate immediately formed and the mixture was stirred at room temperature

for 1 h. The product was filtered, washed several times with methanol and dried in the oven at 80 °C overnight (0.84 g, 87 %).

^{1}H NMR (400.13 MHz, DMSO d6, 25 ºC) δ = 9.10 (s, 1H), 7.77 (s, 1H), 7.70 (s, 1H), 4.19 (t, J = 8.0 Hz, 2H), 3.86 (s, 3H), 1.81 (m, 2H), 1.28 (t, J = 8.0 Hz, 2H), 0.93 (t, J = 8.0 Hz, 3H) ppm. **^{31}P NMR** (162 MHz, CD_3CN, 25 ºC) δ = -2.38 ppm. **Selected FTIR** (cm^{-1}, KBr): 3146 (m); 3110 (w), 3089 (w) (arν(C-H)), 2959 (m); 2931 (w); 2867 (w); 1602 (w); 1564 (m); 1462 (m); 1425 (w); 1379 (w); 1334 (w); 1165 (s); 1105 (w), 1062 (vs), 956 (vs), 878 (vs), 796 (s), 648 (m); 620 (s); 504 (s); 464 (w). Anal. calcd. for $(C_8H_{15}N_2)_3PMo_{12}O_{40}$ (2239.88): C, 13.20; H, 1.99; N, 3.72; Found: C, 13.19; H, 2.01; N, 3.72.

2.5. Synthesis of N-(3-trimethoxysilylpropyl)pyridinium iodide

The synthesis was performed in 1:1 molar ratio, by heating 3-iodopropyltrimethoxysilane (0.404 mL, 1 mmol) with pyridine (0.167 mL, 1 mmol) at 80 ºC for 3 h under nitrogen atmosphere. The product was washed with diethyl ether (3x20 mL). The product was obtained as a viscous brownish yellow oil after dried in vacuum for 2 h (0.72 g, 94 %). [35]

^{1}H NMR (400.13 MHz, CDCl3, 25 ºC) δ = 9.36 (d, J = 6.0 Hz, 2H), 8.60 (t, J = 7.8 Hz, 1H), 8.18 (t, J = 6.6 Hz, 2H), 4.98 (t, J = 7.2 Hz, 2H), 3.59 (s, 9H), 2.18 (m, 2H), 0.73 (t, J = 8.0 Hz, 2H) ppm. **Selected FTIR** (NaCl cell,/cm^{-1}): 3441 (br); 3128 (m); 3028 (w); 2943 (m); 2839 (s); 1632 (vs); 1579 (m); 1486 (vs); 1460 (w); 1413 (w); 1350 (w); 1317 (m); 1245 (w); 1191 (s); 1079 (vs); 889 (w); 815 (s); 776 (s); 682 (vs); 646 (w).

2.6. Preparation of Mesoporous Silica Nanoparticles (MSNs)

The mesoporous nanosilica support was prepared following the method described by Bouchoucha *et al.*.[23] A mixture containing CTAB (0.663 g), Pluronic F127 (2.68 g) and TEA (15.64 g) in EtOH (57 mL), and water (125 mL) was prepared and stirred for 24 h at room temperature. Afterwards, TEOS (2.56 mL was added under vigorous stirring for 1 min in a global molar ratio TEOS : CTAB : F127 : H_2O : EtOH : TEA of 1 : 0.16 : 0.017 : 605 : 84 : 9.16. The mixture was aged under static conditions for 24 h followed by addition of EtOH (100 mL) to promote precipitation. The resulting nanoparticles were collected by centrifugation, washed with water and dried at 80 °C. The dried nanoparticles were calcined in air at 550 °C for 5 h at a heating rate of 1 °C/min.

2.7. Preparation of $PMo_{12}O_{40}$@PPy-MSN

Calcined MSN (0.40 g) was heated at 150 °C under reduced pressure for 2 h to remove the physisorbed water. After cooling down to room temperature, an excess of 1-(3-trimethoxysilylpropyl)-pyridinium (PPy) iodide in acetonitrile (20 mL) was added and the mixture was stirred under reflux and nitrogen atmosphere for 48 h. The resultant powder was centrifuged at 5000 rpm, washed with acetonitrile and chloroform several times and dried in the oven at 80 °C. Afterwards, an anion exchange was performed to change iodide by hydroxide anions following the method of Udayakumar *et al*.[36] The previously functionalized MSN (0.40 g) was treated with a NaOH solution (0.025 M) for 2 h, and then centrifuged and washed several times with distilled water. The product was dried in an oven at 80 °C.

PPy-OH-MSN: ^{1}H NMR (400.13 MHz, D_2O + NaOH, rt) δ = 8.68 (d, 1H), 8.37 (t, J = 4.0 Hz, 1H), 7.89 (d, 2H), 4.40 (t, 2H), 1.91 (m, 2H), 0.21 (t, 2H) ppm. Selected FT-IR (cm^{-1}, KBr): 3443 (br); 3153 (sh), 3097 (sh), 3072 (sh), 2958 (sh), 2929 (sh), 2854 (sh), 1638 (m); 1556 (w), 1541 (w), 1490 (m), 1456 (w), 1415 (w), 1375 (w), 1090 (s); 960 (w); 796 (m); 678 (m); 533 (w); 463 (s).

The $PMo_{12}O_{40}$@PPy-MSN composite was prepared by mixing a suspension of PPy-MSN (0.130 g) with a solution of $H_3[PMo_{12}O_{40}]$ (0.07 mmol in 15 mL of methanol) and stirring at room temperature for 48 h. The solid was centrifuged and washed several times with methanol and dried in the oven at 80 °C. Anal. Found (%): C, 8.58; N, 1.03; H, 1.65; Mo, 2.9.; loading of PMo_{12}: 0.025 mmol per g and ratio of C_3Py/POM ≈ 30. Selected FT-IR (cm^{-1}, KBr): 3441 (br), 3145 (sh), 3097 (sh), 3074 (sh), 2956 (w), 2924 (w), 2852 (sh), 1636 (m), 1558 (w), 1541 (w), 1510 (w), 1498 (w), 1489 (m), 1456 (w), 1417 (w), 1384 (w), 1351 (w), 1091 (vs), 960 (m), 919 (sh), 891 (sh), 801 (m), 680 (w), 551 (sh), 465 (s).

2.8. Extractive and catalytic Oxidative desulfurization processes (ECODS)

The ECODS studies were performed using a model diesel containing the most refractory sulfur-compounds present in real diesel, namely: 1- benzothiophene (1-BT), dibenzothiophene (DBT), 4-

methyldibenzothiophene (4-MDBT) and 4,6- dimehtyldibenzothiophene (4,6-DMDBT). All the experiments were carried out under air (atmospheric pressure) in a closed borosilicate 5 mL reaction vessel, equipped with a magnetic stirrer and immersed in a thermostatically controlled liquid paraffin bath at 70 °C. The catalytic oxidative step was performed in the presence of a polar extraction solvent, immiscible with the model diesel phase with equal volume of model diesel and extraction solvent. The ionic liquid (IL), 1-butyl-3- methylimidazolium hexafluorophosphate ($BMIMPF_6$) and acetonitrile (MeCN) were used as extraction solvents. These solvents acted as extraction solvents of sulfur compounds and also as an oxidative reaction medium. The oxidation of the sulfur compounds only occurred in the presence of a catalyst and an oxidant, where H_2O_2 (aq. 30%) was used. $[BPy]_3[PMo_{12}O_{40}]$ and $[BMIM]_3[PMo_{12}O_{40}]$ dissolved in MeCN, but showed to be insoluble in ionic liquid solvent. In all ECODS systems 3 μmol of each compound was used. The heterogeneous catalyst $PMo_{12}O_{40}$@PPy-MSN was also studied, using 120 mg that contains 3 μmol of $[PMo_{12}O_{40}]^{3-}$ active center. In a typical experiment, 0.75 mL of model diesel (containing a total sulfur concentration of 2350 ppm in n-octane) and 0.75 mL of $[BMIM][PF_6]$ were added to the catalyst. An initial extraction of sulfur compounds from model diesel to the IL phase occurred by only stirring the both immiscible phase for 10 min at 70 °C. The catalytic step of the process is then initiated by the addition of H_2O_2 (75 μL, 0.64 mmol). The sulfur content in the model diesel phase was periodically quantified by GC analysis using tetradecane as standard. Using the heterogeneous catalyst, recycle experiments were performed by adding a new portions of model diesel, oxidant and $[BMIM][PF_6]$ extraction solvent, at the end of each ECODS cycle. The solid catalyst was not washed between cycles. After three cycles, the solid was isolated from the ECODS process, followed by washing and dry to be characterized after catalytic use.

3. Results and discussion

3.1. Synthesis and Characterization

The salts $[BPy]_3[PMo_{12}O_{40}]$ and $[BMIM]_3[PMo_{12}O_{40}]$ were prepared from an acid-base reaction using $H_3PMo_{12}O_{40}$ and the hydroxide forms of 1-butylpyridinium and 1-butyl-3-methylimidazolium, respectively. The hydroxide forms were previously prepared from the corresponding chlorides ionic liquids by exchange of the chloride to the hydroxide using an ion exchange resin Amberlist (in the OH form). The homogeneous catalysts were characterized by

elemental analyses, FT-IR, ^{1}H and ^{31}P NMR spectroscopies. CHN elemental analyses confirm the expected molecular formulas of both compounds. The infrared spectrum of $[BPy]_3[PMo_{12}O_{40}]$ contains weak bands at 3124, 3080 and 3063 cm^{-1} corresponding to ν(C-H) aromatic vibrations, at 2963, 2929 and 2869 cm^{-1} attributed to the ν(C-H) of the aliphatic chain, a strong band at 1632 cm^{-1} corresponding to ν(C=N) vibrations that is typical of the quaternary nitrogen atom in a heterocyclic ring. Several weak/medium bands in the range 1580-1100 cm^{-1} are observed due to aromatic ν(C-N), ν(C-C) and also due δ(C-H) vibrations. A strong band at 1482 cm^{-1} is attributed to the conjugation of ν(C=C) and ν(C=N) bonds and is also typical of pyridinium salts and the strong one at 682 cm^{-1} corresponds to the aromatic out-of- plane hydrogen deformation.[37, 38] The presence of $PMo_{12}O_{40}^{3-}$ is corroborated by four strong bands at 1063, 956, 878 and 795 cm^{-1} corresponding to $\nu_{as}(P\text{-}O_a)$, $\nu_{as}(Mo\text{-}O_d)$, $\nu_{as}(Mo\text{-}O_b\text{-}Mo)$ and $\nu_{as}(Mo\text{-}O_c\text{-}Mo)$, respectively.[39, 40]The bands observed at the infrared spectrum of $[BMIM]_3[PMo_{12}O_{40}]$ are in accordance with the literature confirming the presence of the $[BMIM]^+$ cation and the Keggin anion.[41]

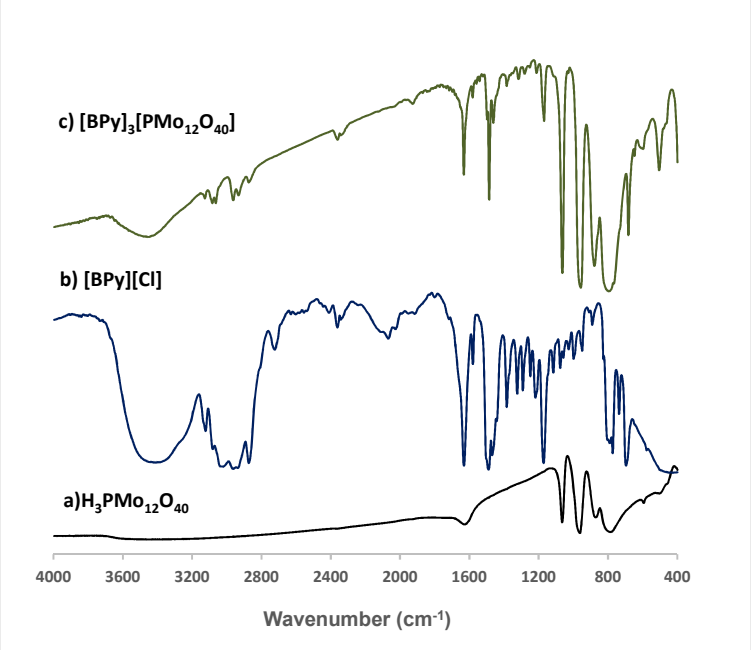

Figure 1- . FT-IR spectra of a) phosphomolybdic acid $H_3PMo_{12}O_{40}$, b) [BPy][Cl] and c) Ionic-Liquid phosphomolybdate $[BPy]_3[PMo_{12}O_{40}]$.

^{1}H NMR spectra of the catalysts are presented in Figure S1 (in Supporting information, SI) and in both is possible to identify the protons from the aliphatic chains and from the aromatic imidazolium or pyridinium rings. In the case of $[BMIM]_3[PMo_{12}O_{40}]$, the proton chemical shifts of imidazolium cation are found at 9.10, 7.77, 7.70 and 3.86 ppm. It also can be observed the protons corresponding to the methyl groups at 4.19, and at 1.81, 1.28 and 0.93 ppm, those attributed to the butyl chain. The spectrum of $[BPy]_3[PMo_{12}O_{40}]$ contains the protons of the pyridinium ring at 9.10, 8.63 and 8.19 ppm and those from the butyl aliphatic chain at 4.63, 1.95, 1.31 and 0.94 ppm.

Figure 2 shows the ^{31}P MAS NMR spectra in CD_3CN of the catalysts that contain a sharp peak at -2.09 ppm for $[BPy]_3[PMo_{12}O_{40}]$ and at -2.38 ppm for $[BMIM]_3[PMo_{12}O_{40}]$. These results were closed to the obtained for other Keggin phosphomolybdate structure containing different organic cations.[33, 42]

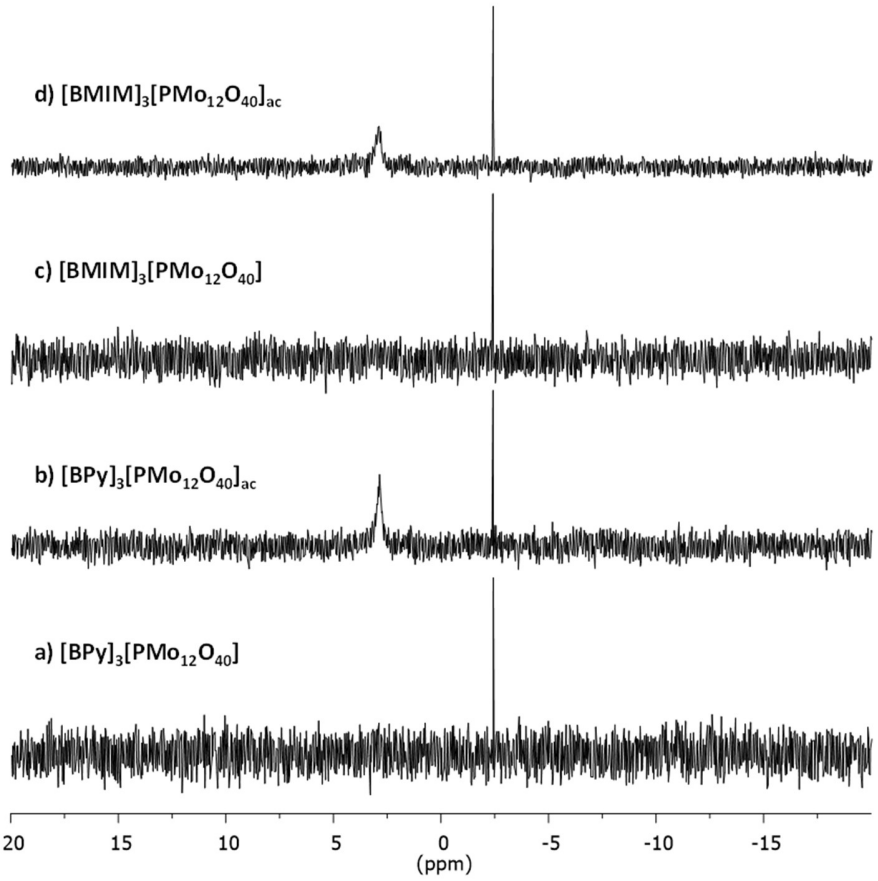

Figure 2: ^{31}P NMR spectra in CD_3CN for the Ionic-Liquid phosphomolybdates $[BPy]_3[PMo_{12}O_{40}]$ and $[BMIM]_3[PMo_{12}O_{40}]$, before and after catalytic use (abbreviated as ac, corresponding to soluble phosphomolybdate compounds in ECODS).

The heterogeneous catalyst $PMo_{12}O_{40}$@PPy-MSN was prepared according to the scheme 1. First the pristine MSNs was functionalized with 1-(3-trimethoxysilylpropyl)-pyridinium iodide (previously prepared) and then the iodide anions were exchanged by OH^- anions using a NaOH solution (0.025M) following the method described by Udayakumar *et al*..[36]To this last material, phosphomolybdic acid was added and through an acid-base reaction the final composite was obtained. The intermediate support material PPy-OH-MSN was characterized by FTIR and ^1H NMR spectroscopies to confirm the presence of the anchored cation (solution ^1H NMR was used following the method described by Crucho *et al*.). The infrared spectrum of PPy-OH-MSN contains the strong bands characteristic of silica-type materials at 1064, 796 and 463 cm^{-1} attributed to ν_{as}(Si–O–Si), ν_s(Si–O–Si) and δ(O–Si–O) vibrational modes, respectively. Beyond these bands, it shows several weak bands from the functionalized pyridinium cation in the region 3160-3000 cm^{-1} (ν(C-H) aromatic vibrations), 2960-2850 cm^{-1} (ν(C-H) of the aliphatic chain), and 1500-1300 cm^{-1} (ν(C-N), ν(C-C), δ(C-H)) (Figure 3). ^1H NMR spectrum of this material exhibits the chemical shifts of the pyridinium protons at 8.68, 8.37, and 7.89 ppm and the corresponding signals of the propyl chain at 4.40, 1.91 and 0.21 ppm (see Figure. S2 in SI).

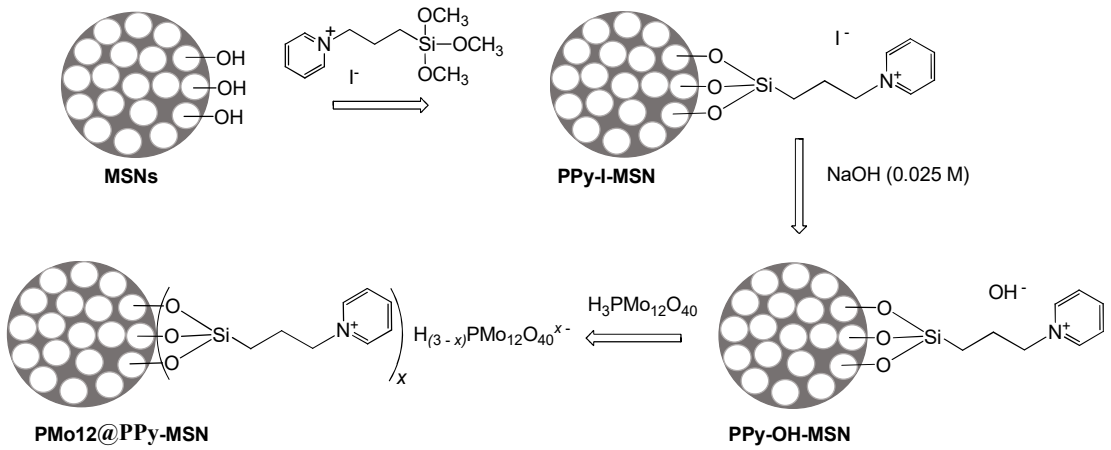

Scheme 1: Schematic representation of the method used to prepare the final heterogeneous catalyst $PMo_{12}O_{40}$@PPy-MSN

The final composite was characterized by elemental CHN and Mo analyses, FTIR, ^{13}C CP MAS and ^{31}P MAS solid state NMR spectroscopies. Elemental analyses revealed a loading of 0.7 mmol of pyridinium cations and 0.025 mmol of $PMo_{12}O_{40}^{3-}$ per g of material. The FTIR spectrum of $PMo_{12}O_{40}$@PPy-MSN, in addition to the bands corresponding to the functionalized cation, displays one band at 960 (this band overlap the one from precursor PPy-OH-MSN which corresponds to the ν(Si-OH) but that is less pronounced) and a shoulder at 891 cm^{-1} that can be ascribed to the ν_{as}(Mo-O_d) and ν_{as}(Mo-O_b-Mo) vibrational modes of the phosphomolybdate anion, respectively (Figure 3).^{13}C CP MAS NMR spectrum contains three peaks corresponding to the aliphatic propyl carbon atoms at 10.6, 23.1 and 45.3 ppm (Figure 4, left) and two peaks in the aromatic region at 130.7 and 146.5 ppm assigned to the pyridium carbon atoms. ^{31}P MAS spectrum exhibits one peak at -3.84 ppm attributed to $PMo_{12}O_{40}$ anion (Figure 4, right).

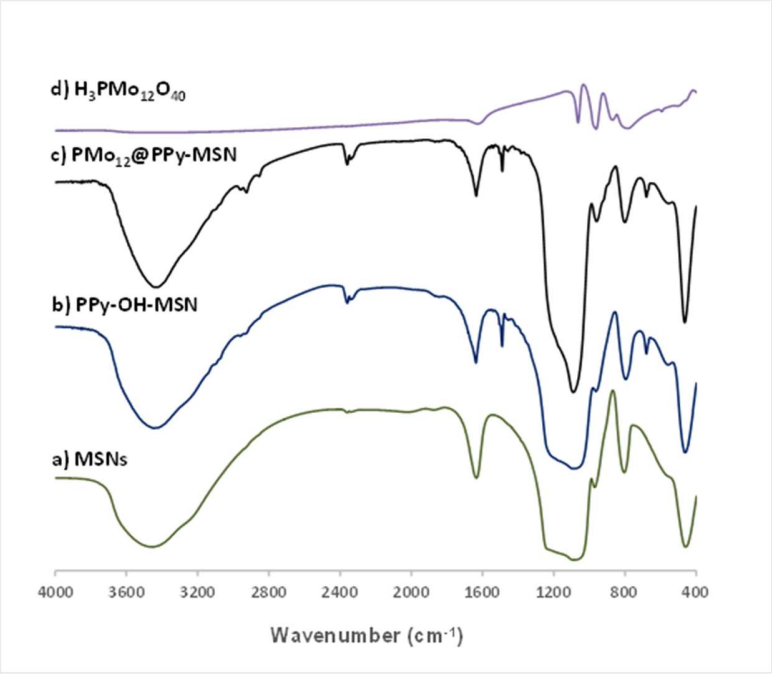

Figure 3- FT-IR spectra of the supports a) calcinated MSNs, b) PPy-OH-MSN and the composite c) $PMo_{12}O_{40}$@PPy-MSN and of phosphomolybdic acid d) $H_3PMo_{12}O_{40}$.

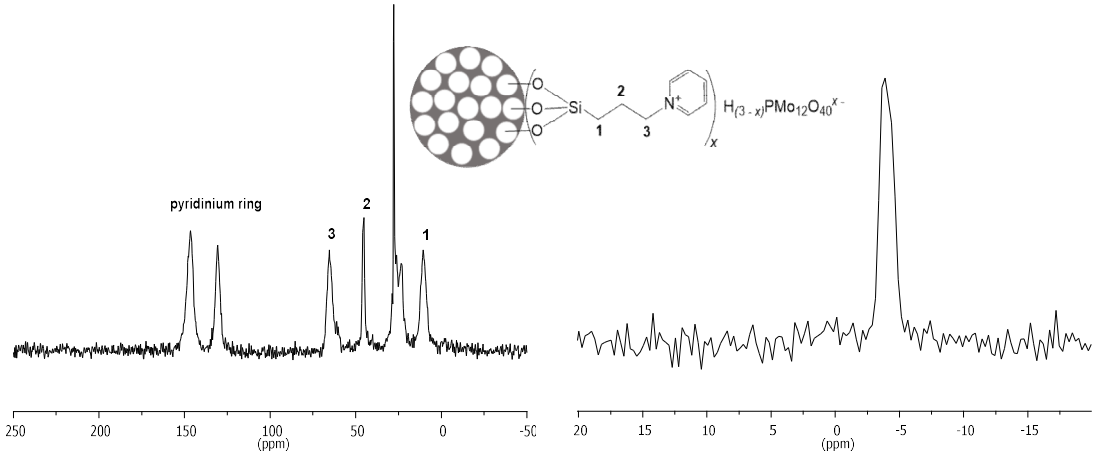

Figure 4. ^{13}C CP MAS (on left) and ^{31}P CP MAS (on left) for the composite $PMo_{12}O_{40}$@PPy-MSN.

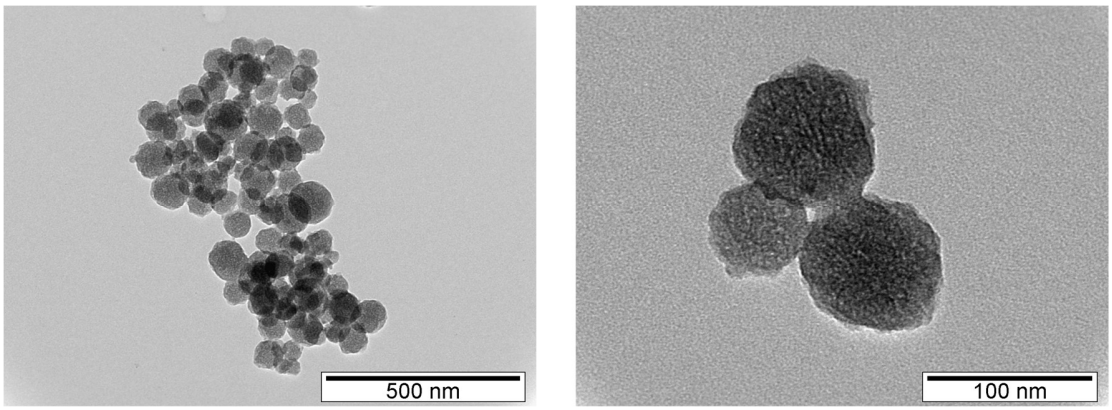

Figure 5. TEM images of the heterogeneous catalyst $PMo_{12}O_{40}$@PPy-MSN

$PMo_{12}O_{40}$@PPy-MSN was also characterized by transmission electron microscopy (Figure 5) and the images show that the composite are constituted by spherical porous nanoparticles with a size distribution in the range of 50-80 nm with some aggregation.

3.2. Extractive and Catalytic Oxidative desulfurization systems (ECODS)

The ionic-liquid based phosphomolybdates [BMIM]PMo_{12} and [BPy]PMo_{12} and the composite PMo_{12}@PPy-MSN were used as catalysts in an extractive and catalytic oxidative desulfurization

system (ECODS) using a model diesel composed by the most refractory sulfur compounds in real diesels, namely, 1-benzothiophene (1-BT), dibenzothiophene (DBT), 4- methyldibenzothiophene (4-MDBT) and 4,6-dimethyldibenzothiophene (4,6-DMDBT) in *n*-octane. This model diesel has a sulfur concentration of approximately 500 ppm for each compound and a total of 2350 ppm of sulfur. The ECODS process begins with an initial extraction step by stirring the diesel phase with a polar immiscible phase during 10 min at 70 ◦C. This first step of ECODS process promotes the transfer of the sulfur compounds from the model diesel to the polar phase. In this studies an ionic liquid ([BMIM][PF_6) were used. The second step of the desulfurization process is initiated by the addition of H_2O_2 oxidant, using a ratio H_2O_2/S = 11. This step corresponds to the oxidative catalytic step, where the sulfur compounds in the [BMIM]PF_6 phase are oxidized to sulfoxides and/or sulfones. This leads to a continuous transfer of non-oxidized sulfur compounds from the model diesel to the ionic liquid phase. The order of each sulfur component, at the end of initial extraction step was the following: BT > DBT > 4-MDBT > 4,6-DMDBT (Table 1). These results are explained by the different molecular diameters, as well as by the steric hindrance of the methyl groups in DBT derivatives. [14, 16, 42, 43]

Table 1. Individual desulfurization percentages from the model diesel to the extraction phase using $[BPy]_3[PMo_{12}O_{40}]$, $[BMIM]_3[PMo_{12}O_{40}]$ and PMo_{12}@PPy-MSN catalysts.

	Initial Desulfurization (%)			
Catalyst	**1-BT**	**DBT**	**4-MDBT**	**4,6-DMDBT**
$[BPy]_3[PMo_{12}O_{40}]$	42	31	19	4
$[BMIM]_3[PMo_{12}O_{40}]$	46	38	27	18
$PMo_{12}O_{40}$@PPy-MSN	54	53	38	28

After the initial extraction step, the sulfur transfer equilibrium between the model diesel and ionic liquid phases was achieved, and the removal of more sulfur compounds from model diesel only could occurred by the oxidation of the sulfur compounds present in the [BMIM][PF_6] phase, i.e. after the addition of H_2O_2 oxidant in the presence of the phosphomolybdate catalyst. During the catalytic oxidative desulfurization step the no-oxidized sulfur compounds are oxidized in the corresponding sulfone and/or sulfoxides. The oxidation of sulfur compounds must occur more

extensively in the [BMIM][PF_6] phase since the oxidant has more affinity with this solvent than with the model diesel phase.

The ionic-liquid phosphomolybdates [BPy]$_3$[$PMo_{12}O_{40}$] and [BMIM]$_3$[$PMo_{12}O_{40}$] are not dissolved in the [BMIM][PF_6] phase, behaving as heterogeneous catalysts. The desulfurization profiles obtained using these two catalysts are presented in Figure 6. It is possible to observe that both ionic liquid catalysts present similar desulfurization profile and only a slightly higher desulfurization efficiency can be found for [BPy]$_3$[$PMo_{12}O_{40}$] during the first hour of reaction. After this time complete desulfurization was achieved in both ECODS systems. The difference of catalytic activity observed during the first hour indicates that the reactivity of these catalysts depends on the type of the counter-cation, in this case 1-butyl-3-methylimidazolium ($[BMIM]^+$) and butylpyridinium ($[BPy]^+$). It is reported in the literature by Fugita, *et al*. that these cations present some influence in the catalyst performance, varying in the order: $[BPy]^+ > [BMIM]^+$. [44]

When the ECODS experiments were performed using acetonitrile instead of [BMIM][PF_6], the phosphomolybdates [BPy]$_3$[$PMo_{12}O_{40}$] and [BMIM]$_3$[$PMo_{12}O_{40}$] behaved as homogeneous catalysts, since these were completely dissolved in this solvent. In this case, after the first hour of reaction, complete desulfurization was not achieved (desulfurization efficiency of 83%, Figure S3 in SI). The superior desulfurization performance using [BMIM][PF_6] solvent against organic solvents in ECODS processes has been previously reported. [43, 45]

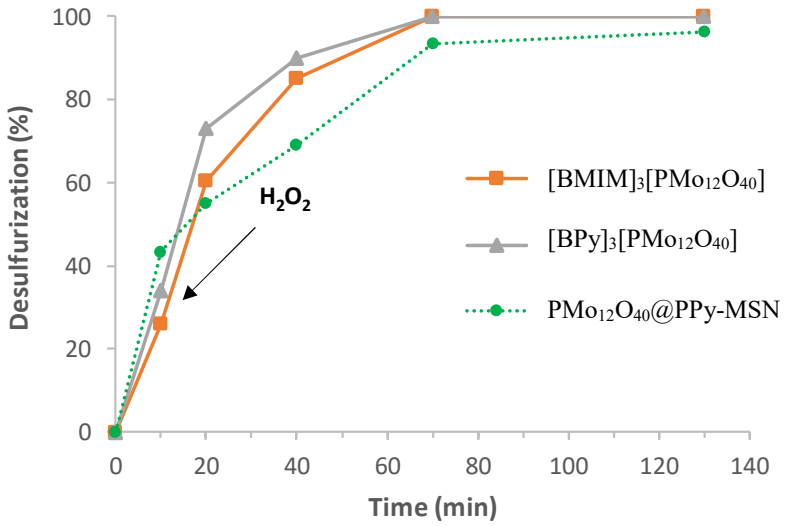

Figure 6- Kinetic desulfurization profiles for ECODS process 1:1 model diesel/ [BMIM][PF_6], catalyzed by $[BPy]_3[PMo_{12}O_{40}]$ and $[BMIM]_3[PMo_{12}O_{40}]$ (3 μmol), using H_2O_2/ S = 11, at 70ºC.

The stability and the heterogeneity of $[BMIM]_3[PMo_{12}O_{40}]$ and $[BPy]_3[PMo_{12}O_{40}]$ catalysts were analyzed by ^{31}P NMR ($[BMIM]_3[PMo_{12}O_{40}]$-ac and $[BPy]_3[PMo_{12}O_{40}]$-ac spectra). The solid catalysts after catalytic use were recovered from the reaction medium and washed with ethanol and dried. Afterwards, these last was dissolved in CD_3CN and the ^{31}P NMR analysis present single peaks at -2.40 ppm and -2.39, that corresponds to the initial prepared $[BPy]_3[PMo_{12}O_{40}]$ and $[BMIM]_3[PMo_{12}O_{40}]$, respectively (spectra not shown). This result indicates that the solid catalyst presents the initial structure and its typical Keggin structure was confirmed. On the other hand, the soluble reaction media using $[BMIM]_3[PMo_{12}O_{40}]$ and $[BPy]_3[PMo_{12}O_{40}]$ were also analyzed by ^{31}P NMR and in this case two single peaks were found at 2.90 and -2.39 ppm, for $[BMIM]_3[PMo_{12}O_{40}]_{ac}$ and 2.87 and -2.40 for $[BPy]_3[PMo_{12}O_{40}]_{ac}$ (Figure 2). These results indicate that the ionic liquid phosphomolybates has some partial dissolution in the ionic liquid medium during catalytic reaction and also identical structural alteration of the Keggin structure may occurred for both compounds (single peaks at 2.90 ppm and 2.87 ppm for $[BMIM]_3[PMo_{12}O_{40}]$ and $[BPy]_3[PMo_{12}O_{40}]$, respectively), probably by their interaction with the oxidant.

To increase the stability of the ionic-liquid $[PMo_{12}O_{40}]^{3-}$ catalyst and to guarantee its heterogeneity, this Keggin phosphomolybdate was immobilized in pyridinium (PPy) functionalized mesoporous silica nanoparticles ($PMo_{12}O_{40}$@PPy-MSN, Scheme 1). Figure 6 compares the desulfurization profile of the composite $PMo_{12}O_{40}$@PPy-MSN and the ionic liquid phosphomolybdate catalysts. The initial extraction of sulfur compounds from model diesel to the [BMIM][PF_6] phase (stirring 10 min at 70 ºC) was slightly higher using the composite material (43% using the composite and 26% and 34% using $[BMIM]_3[PMo_{12}O_{40}]$ and $[BPy]_3[PMo_{12}O_{40}]$, respectively). This must be related to the presence of a higher amount of solid in the ECODS system (120 mg, containing 3 μmol of active $[PMo_{12}O_{40}]^{3-}$ catalyst), promoting by some sulfur adsorption on MSN surface or even by increasing the liquid-liquid contact between model diesel and ionic liquid phases. During the oxidative catalytic step (after the first 10 min), the desulfurization increased rapidly and after only 1 h 93% was achieved remaining only 1-BT in the model diesel. The desulfurization increased more slowly after the first hour: after 2 h was found

96% and after 3 h 98% (39 ppm of sulfur attributed to 1-BT). In fact, it is well reported in the literature the higher difficulty to oxidize 1-BT due to the lower electron density on its sulfur atom, when compared with the other studied compounds and consequent lower reactivity [46-48]. The other studied sulfur compounds (DBT, 4-MDBT and 4,6-DMDBT) exhibit similar electron densities on the sulfur atom and therefore their oxidation can only be distinct by the steric hindrance promoted by the methyl groups. The MSN support has also been tested under identical conditions, presenting a negligible catalytic activity.

The reusability of the ECODS model diesel/[BMIM][PF_6] system catalyzed by the composite $PMo_{12}O_{40}$@PPy-MSN was investigated for three consecutive cycles. After 3 h of oxidative desulfurization, the solid catalyst remained in the ionic liquid phase and the model diesel could be easily removed from the system. The ionic liquid phase containing the heterogeneous catalyst was then reused in a new ECODS cycle. The new ECODS cycle was prepared by simple addition of a new portion of sulfurized model diesel and 75 μL of oxidant. The reuse of the ionic-liquid phase and the solid catalyst creates a more sustainable ECODS process, reducing costs and residual wastes. Figure 7 presents the desulfurization profile for three consecutive ECODS cycles using the same sample of PMo_{12}@PPy-MSN and [BMIM][PF_6]. The desulfurization profile of the three consecutive ECODS cycles is similar, indicating that the composite PMo_{12}@PPy-MSN maintained its oxidative activity. For all the three ECODS cycles near complete desulfurization was achieved after 3 h, remaining a vestigial amount of 1-BT in the model diesel. The DBT, 4-MDBT and 4,6-DMDBT were complete desulfurize after de 1 h of oxidation. It is also important to note that the increasing concentration of oxidized products in the $BMIMPF_6$ phase over the three consecutive ECODS cycles was observed by increasing the amount of formed white solid in this phase over the various cycles. However, this did not contribute to the loss of desulfurization performance and ultra-low sulfur model diesel was easily produced in consecutive cycles. to remove the sulfones after the three consecutive desulfurization cycles. After these consecutive cycles, the heterogeneous catalyst was recovered by centrifugation and the $BMIMPF_6$ phase was cleaned with a mixture of 1:1 (v/v) ethyl acetate and diethyl ether to extract the dissolved sulfones in this phase. Furthermore, the used solvents (ethyl acetate and diethyl ether) could be recovered by distillation and the white solid sulfones were isolated.

the solid catalyst and the white precipitate sulfones were separated from the IL phase. The resulting IL phase was then treated with a mixture to the IL phase

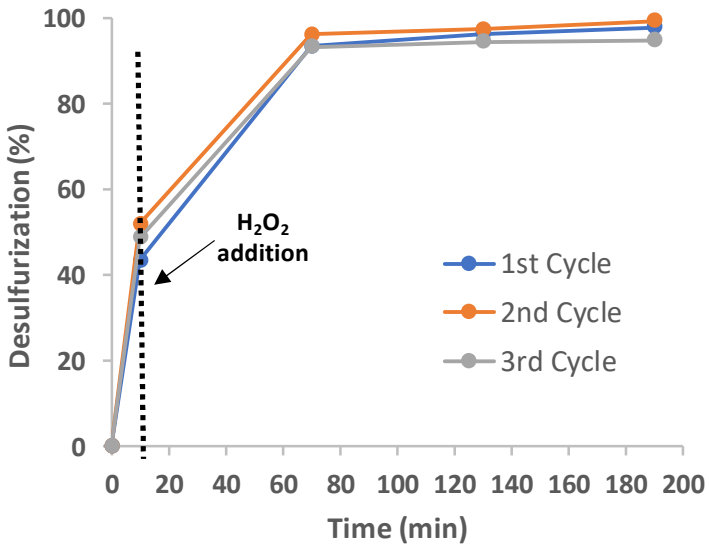

Figure 7- Reusability of the ECODS (1:1 model diesel/[BMIM][PF_6]) process catalyzed by $PMo_{12}O_{40}$@PPy-MSN composite (containing 3 µmol of active $[PMo_{12}O_{40}]^{3-}$), using H_2O_2 as oxidant (75 µL, using H_2O_2/ S = 11), at 70 °C.

The desulfurization efficiency obtained by $PMo_{12}O_{40}$@PPy-MSN heterogeneous catalyst is similar to the previous obtained by our research group using related heterogeneous catalysts under identical experimental conditions.[33] The advantage showed by $PMo_{12}O_{40}$@PPy-MSN is its higher stability between consecutive reused ECODS cycles. This must be related to the immobilization of the phosphomolybdate in the surface of the functionalized MSN. In this work, a propylpyridinium (PPy) functional group was strategically used, instead of the tributylammonium (TBA^+) and trimethylammonium (TMA^+) used previously.[33]

3.3. Stability of $PMo_{12}O_{40}$@PPy-MSN after ECODS

The stability of the composite $PMo_{12}O_{40}$@PPy-MSN, after three consecutive ECODS cycles, was investigated by various characterization techniques, such as ^{31}P NMR, FT-IR and SEM/EDS.

The presence of active catalytic center $[PMo_{12}O_{40}]^{3-}$ in the reaction medium, after solid catalyst removal, was investigated. The reaction medium in [BMIM][PF_6] was diluted in CD_3CN and ^{31}P NMR analysis was performed. Even after 24 h of analysis, no single peak attributed to Keggin-type phosphomolybdate or its derivatives were detected. This result suggests the absence of active leaching species from the surface of PPy-MSN support.

The ATR-FTIR spectrum of composite after catalytic use $PMo_{12}O_{40}$@PPy-MSN-ac (ac stands for after catalysis, Figure S4 in SI) can be compared to the same before ECODS application in Figure 3, where similar main bands are exhibited around 960 (ν(Si-OH) and ν_{as}(Mo-O_d)) and 890 cm^{-1} (ν_{as}(Mo-O_b-Mo), which is consistent with the structural retention of the POM anion after catalytic use. [33, 42]

The morphology and chemical composition of $PMo_{12}O_{40}$@PPy-MSN was analyzed by electronic microscopy analysis before and after catalytic use during three ECODS cycles (Figure 8). The nanoparticles morphology is preserved after the immobilization of the active $[PMo_{12}O_{40}]^{3-}$ center and after the catalytic used for three consecutive cycles. In fact, the composite is still composed by the same type of nanoparticles without changing their shape or size. The presence of $[PMo_{12}O_{40}]^{3-}$ before and after catalytic use could be confirmed by EDS analysis (Figure 9). The spectra in Figure 9 reveal the presence of silicon from the support and the presence of molybdenum from the phosphomolybdate. The presence of fluorine and phosphorus in the composite after catalytic use indicate that same ionic liquid [BMIM][PF_6] must be present in the solid catalyst after ECODS application. The leaching of active species $[PMo_{12}O_{40}]^{3-}$ from the composite $PMo_{12}O_{40}$@PPy-MSN during the three consecutive ECODS cycles was investigated by the ratio Si/Mo, performed by EDS analysis. Before catalytic use the ratio Si/Mo was 9,8 and after recycling study the same ratio was 9,3. This result suggests that the loss of active center to the reaction medium after three consecutive ECODS cycles was negligible (5%), confirming the stability of $PMo_{12}O_{40}$@PPy-MSN heterogeneous catalyst.

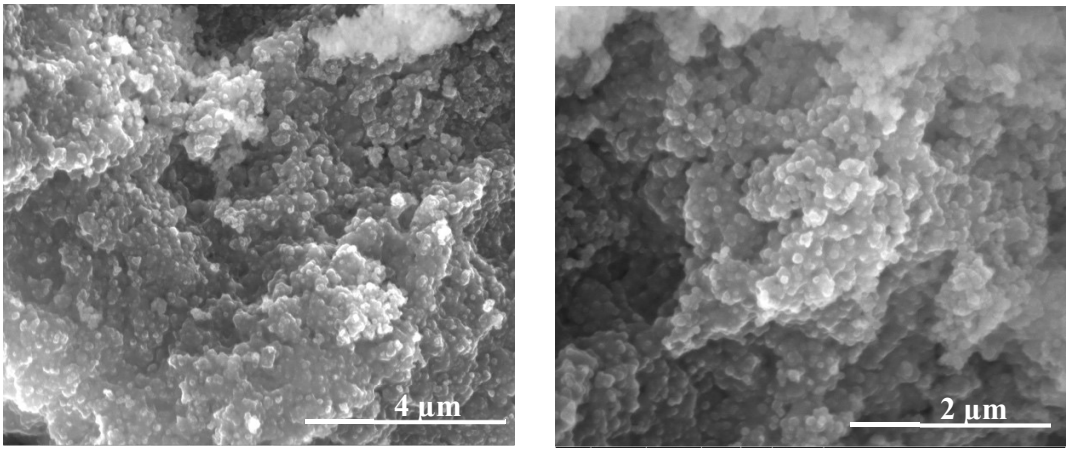

Figure 8- SEM images of the $PMo_{12}O_{40}$@PPy-MSN composite material before (left) and after (right) catalytic use ($PMo_{12}O_{40}$@PPy-MSN-ac) at different magnifications: (left) ×25,000 and (right) ×50,000.

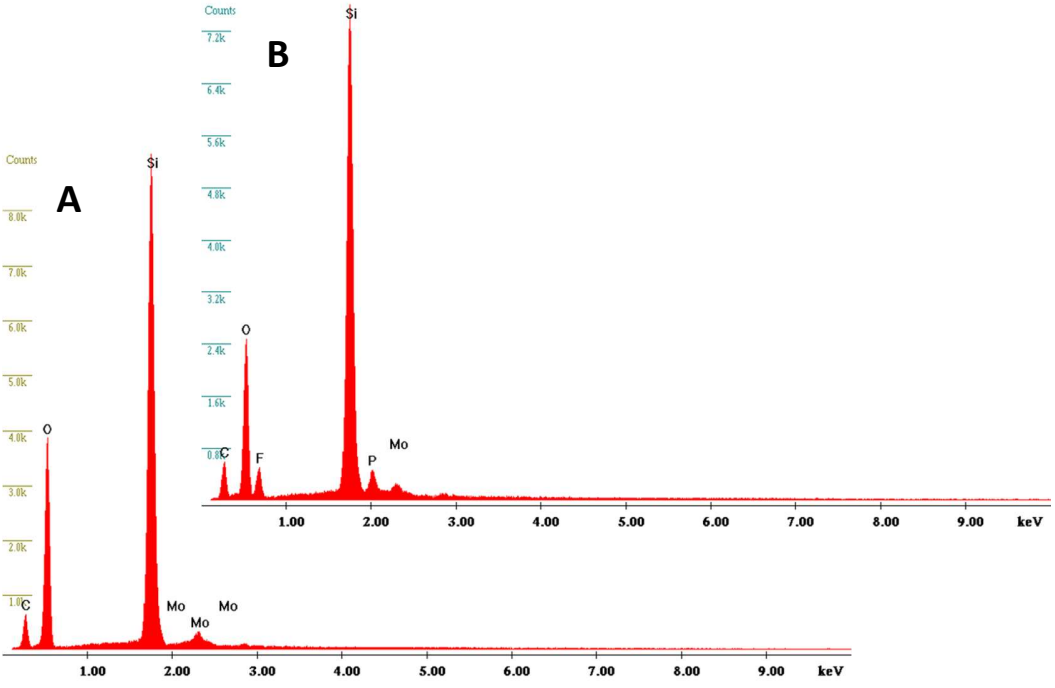

Figure 9- EDS spectra of the $PMo_{12}O_{40}$@PPy-MSN composite material (A) before and (B) after catalytic use during three consecutive ECODS cycles.

4. Conclusion

Two different ionic liquid phosphomolybdates, containing 1-butylpyridinium ($[BPy]_3[PMo_{12}O_{40}]$) and 1-butyl-3-methylimidazolium ($[BMIM]_3[PMo_{12}O_{40}]$) were prepared and used as catalysts for the oxidative desulfurization of a multicomponent model diesel. The catalytic studies were performed using biphasic desulfurization systems (1:1 model diesel/extraction solvent, using acetonitrile and an ionic liquid $[BMIM][PF_6]$ as solvent). An initial extraction of the sulfur compounds from diesel phase to the extraction phase was performed during 10 min at 70 ºC. Afterwards, the catalytic oxidative desulfurization step was performed by the addition of H_2O_2 oxidant (H_2O_2/S = 11). Higher desulfurization and higher oxidative catalytic efficiency were achieved using the ionic liquid extraction solvent. In this case, complete desulfurization was achieved after the first hour using both phosphomolybdate catalysts. Using model diesel/$[BMIM][PF_6]$ system, the $[BPy]_3[PMo_{12}O_{40}]$ and $[BMIM]_3[PMo_{12}O_{40}]$ showed to be partially soluble. Their stability study indicated that the solid part maintained their initial Keggin structure; however, the soluble phosphomolybdate species presented some decomposition, probably promoted by their interaction in the H_2O_2 oxidant. To guarantee the heterogeneity of the catalyst and increase its stability, the $[PMo_{12}O_{40}]^{3-}$ active center was immobilized in a propylpyridinium functionalized mesoporous silica nanoparticles ($PMo_{12}O_{40}$@PPy-MSN). This catalytic composite showed slightly lower activity than the previous ionic liquid phosphomolybdates, mainly during the first hour of reaction, since at this time 93% of desulfurization was achieved, remaining only 1-benzothiophene in the model diesel phase. Near complete desulfurization was achieved after 3 h (98% of desulfurization, 39 ppm of 1-BT). Contrarious to ionic liquid phosphomolybdates, the stability of the composite $PMo_{12}O_{40}$@PPy-MSN was confirmed by various techniques and high recycle capacity was found.

Acknowledgements

This work was partly funded through the projects REQUIMTE-LAQV [FCT (Fundação para a Ciência e a Tecnologia) Ref. LAQV, REQUIMTE (POCI-01-0145-FEDER-007265, UID/QUI/50006/2013)] and CENIMAT, I3N (POCI-01-0145-FEDER-007688, UID/CTM/50025/2013), financed by national funds through the FCT/MEC and when appropriate co-financed by the Fundo Europeu de Desenvolvimento Regional (FEDER) under the PT2020 Partnership Agreement. This work is funded by national funds (OE), through FCT – Fundação

para a Ciência e a Tecnologia. European Social Fund through the program POPH of QREN. The authors also acknowledge the Portuguese Nuclear Magnetic Resonance Network (PTNMR).

Appendix A. Suplementary data

Supplementary data related to this article can be found in …

References

[1] A. Samokhvalov, Desulfurization of Real and Model Liquid Fuels Using Light: Photocatalysis and Photochemistry, Catalysis Reviews, 54 (2012) 281-343.

[2] C.M. Granadeiro, S.O. Ribeiro, M. Karmaoui, R. Valenca, J.C. Ribeiro, B. de Castro, L. Cunha-Silva, S.S. Balula, Production of ultra-deep sulfur-free diesels using a sustainable catalytic system based on UiO-66(Zr), Chemical Communications, 51 (2015) 13818-13821.

[3] H. Lu, J. Gao, Z. Jiang, Y. Yang, B. Song, C. Li, Oxidative desulfurization of dibenzothiophene with molecular oxygen using emulsion catalysis, Chemical Communications, (2007) 150-152.

[4] H. Lü, Y. Zhang, Z. Jiang, C. Li, Aerobic oxidative desulfurization of benzothiophene, dibenzothiophene and 4,6-dimethyldibenzothiophene using an Anderson-type catalyst [(C18H37)2N(CH3)2]5[IMo6O24], Green Chemistry, 12 (2010) 1954-1958.

[5] S. Ribeiro, C.M. Granadeiro, P. Silva, F.A. Almeida Paz, F.F. de Biani, L. Cunha-Silva, S.S. Balula, An efficient oxidative desulfurization process using terbium-polyoxometalate@MIL-101(Cr), Catalysis Science & Technology, 3 (2013) 2404-2414.

[6] J.M. Campos-Martin, M.C. Capel-Sanchez, P. Perez-Presas, J.L.G. Fierro, Oxidative processes of desulfurization of liquid fuels, Journal of Chemical Technology & Biotechnology, 85 (2010) 879-890.

[7] N.D. McNamara, G.T. Neumann, E.T. Masko, J.A. Urban, J.C. Hicks, Catalytic performance and stability of (V) MIL-47 and (Ti) MIL-125 in the oxidative desulfurization of heterocyclic aromatic sulfur compounds, Journal of Catalysis, 305 (2013) 217-226.

[8] Y. Zhang, G. Li, L. Kong, H. Lu, Deep oxidative desulfurization catalyzed by Ti-based metal-organic frameworks, Fuel, 219 (2018) 103-110.

[9] F.S. Mjalli, O.U. Ahmed, T. Al-Wahaibi, Y. Al-Wahaibi, I.M. AlNashef, Deep oxidative desulfurization of liquid fuels, Reviews in Chemical Engineering, 30 (2014) 337-378.
[10] M.R. Maurya, A. Arya, A. Kumar, M.L. Kuznetsov, F. Avecilla, J.C. Pessoa, Polymer-Bound Oxidovanadium(IV) and Dioxidovanadium(V) Complexes As Catalysts for the Oxidative Desulfurization of Model Fuel Diesel, Inorganic Chemistry, 49 (2010) 6586-6600.
[11] B.-b. Shao, L. Shi, X. Meng, Deep Desulfurization of 4,6-Dimethyldienzothiophene by an Ionic Liquids Extraction Coupled with Catalytic Oxidation with a Molybdic Compound, Industrial & Engineering Chemistry Research, 53 (2014) 6655-6663.
[12] L. Liu, C. Chen, X. Hu, T. Mohamood, W. Ma, J. Lin, J. Zhao, A role of ionic liquid as an activator for efficient olefin epoxidation catalyzed by polyoxometalate, New Journal of Chemistry, 32 (2008) 283-289.
[13] F. Mirante, S.O. Ribeiro, B. de Castro, C.M. Granadeiro, S.S. Balula, Sustainable Desulfurization Processes Catalyzed by Titanium-Polyoxometalate@TM-SBA-15, Topics in Catalysis, 60 (2017) 1140-1150.
[14] S. Ribeiro, A.D.S. Barbosa, A.C. Gomes, M. Pillinger, I.S. Gonçalves, L. Cunha-Silva, S.S. Balula, Catalytic oxidative desulfurization systems based on Keggin phosphotungstate and metal-organic framework MIL-101, Fuel Processing Technology, 116 (2013) 350-357.
[15] C.M. Granadeiro, A.D.S. Barbosa, S. Ribeiro, I.C.M.S. Santos, B. de Castro, L. Cunha-Silva, S.S. Balula, Oxidative catalytic versatility of a trivacant polyoxotungstate incorporated into MIL-101(Cr), Catalysis Science & Technology, 4 (2014) 1416-1425.
[16] L.S. Nogueira, S. Ribeiro, C.M. Granadeiro, E. Pereira, G. Feio, L. Cunha-Silva, S.S. Balula, Novel polyoxometalate silica nano-sized spheres: efficient catalysts for olefin oxidation and the deep desulfurization process, Dalton Transactions, 43 (2014) 9518-9528.
[17] D. Julião, A.C. Gomes, M. Pillinger, L. Cunha-Silva, B. de Castro, I.S. Gonçalves, S.S. Balula, Desulfurization of model diesel by extraction/oxidation using a zinc-substituted polyoxometalate as catalyst under homogeneous and heterogeneous (MIL-101(Cr) encapsulated) conditions, Fuel Processing Technology, 131 (2015) 78-86.
[18] C.M. Granadeiro, L.S. Nogueira, D. Juliao, F. Mirante, D. Ananias, S.S. Balula, L. Cunha-Silva, Influence of a porous MOF support on the catalytic performance of Eu-polyoxometalate based materials: desulfurization of a model diesel, Catalysis Science & Technology, 6 (2016) 1515-1522.

[19] F. Mirante, S.O. Ribeiro, B. Castro, C.M. Granadeiro, S.S. Balula, Sustainable Desulfurization Processes Catalyzed by Titanium-Polyoxometalate@TM-SBA-15, Top. Catal., (2017) DOI: 10.1007/s11244-11017-10801-11245.
[20] F. Mirante, L. Dias, M. Silva, S.O. Ribeiro, M.C. Corvo, B. de Castro, C.M. Granadeiro, S.S. Balula, Efficient heterogeneous polyoxometalate-hybrid catalysts for the oxidative desulfurization of fuels, Catalysis Communications, 104 (2018) 1-8.
[21] N. Mizuno, K. Yamaguchi, K. Kamata, Epoxidation of olefins with hydrogen peroxide catalyzed by polyoxometalates, Coordination Chemistry Reviews, 249 (2005) 1944-1956.
[22] S.-S. Wang, G.-Y. Yang, Recent Advances in Polyoxometalate-Catalyzed Reactions, Chemical Reviews, 115 (2015) 4893-4962.
[23] M. Bouchoucha, M.-F. Côté, R. C.-Gaudreault, M.-A. Fortin, F. Kleitz, Size-Controlled Functionalized Mesoporous Silica Nanoparticles for Tunable Drug Release and Enhanced Anti-Tumoral Activity, Chemistry of Materials, 28 (2016) 4243-4258.
[24] L. Chen, G. Zhu, D. Zhang, H. Zhao, M. Guo, W. Shi, S. Qiu, Novel mesoporous silica spheres with ultra-large pore sizes and their application in protein separation, Journal of Materials Chemistry, 19 (2009) 2013-2017.
[25] C.T. Kresge, M.E. Leonowicz, W.J. Roth, J.C. Vartuli, J.S. Beck, Ordered mesoporous molecular sieves synthesized by a liquid-crystal template mechanism, Nature, 359 (1992) 710-712.
[26] A. Feliczak-Guzik, B. Jadach, H. Piotrowska, M. Murias, J. Lulek, I. Nowak, Synthesis and characterization of SBA-16 type mesoporous materials containing amine groups, Microporous and Mesoporous Materials, 220 (2016) 231-238.
[27] D. Y., C. Y., S. Z., L. J., L. C., W. J., L. W., L. C., W. Y., Z. D., Multifunctional mesoporous composite microspheres with well-designed nanostructure: a highly integrated catalyst system, Journal of the American Chemical Society, 132 (2010) 8466-8473.
[28] Y. Wan, Y. Shi, D. Zhao, Designed synthesis of mesoporous solids via nonionic-surfactant-templating approach, Chemical Communications, (2007) 897-926.
[29] M. Mamak, N. Coombs, G. Ozin, Self-Assembling Solid Oxide Fuel Cell Materials: Mesoporous Yttria-Zirconia and Metal-Yttria-Zirconia Solid Solutions, Journal of the American Chemical Society, 122 (2000) 8932-8939.

[30] W. Li, J. Liu, D. Zhao, Mesoporous materials for energy conversion and storage devices, Nature Reviews Materials, 1 (2016).
[31] B.G. Trewyn, I.I. Slowing, S. Giri, H.-T. Chen, V.S.Y. Lin, Synthesis and Functionalization of a Mesoporous Silica Nanoparticle Based on the Sol–Gel Process and Applications in Controlled Release, Accounts of Chemical Research, 40 (2007) 846-853.
[32] D. Rath, S. Rana, K.M. Parida, Organic amine-functionalized silica-based mesoporous materials: an update of syntheses and catalytic applications, RSC Advances, 4 (2014) 57111-57124.
[33] F. Mirante, N. Gomes, L.C. Branco, L. Cunha-Silva, P.L. Almeida, M. Pillinger, S. Gago, C.M. Granadeiro, S.S. Balula, Mesoporous nanosilica-supported polyoxomolybdate as catalysts for sustainable desulfurization, Microporous and Mesoporous Materials, 275 (2019) 163-171.
[34] J.M. Palomino, D.T. Tran, J.L. Hauser, H. Dong, S.R.J. Oliver, Mesoporous silica nanoparticles for high capacity adsorptive desulfurization, Journal of Materials Chemistry A, 2 (2014) 14890-14895.
[35] T.-Y. Cho, S.-G. Yoon, S.S. Sekhon, C.-H. Han, Effect of Ionic Liquids with Different Cations in I-/I3- Redox Electrolyte on the Performance of Dye-sensitized Solar Cells, Bull. Korean Chem. Soc., 32 (2011) 2058.
[36] S. Udayakumar, S.-W. Park, D.-W. Park, B.-S. Choi, Immobilization of ionic liquid on hybrid MCM-41 system for the chemical fixation of carbon dioxide on cyclic carbonate, Catalysis Communications, 9 (2008) 1563-1570.
[37] D. Cook, Vibracional spectra of pyridinium salts, Canadian Journal of Chemistry, 39 (1961) 2009-2024.
[38] M. Katcka, T. Urbanski, T.U.M. Katcka, Bull. L'Cademie Pol. Des Sci. Des Sci. Chim. , XII (1964) 615-621.
[39] C. Rocchiccioli-Deltcheff, M. Fournier, R. Franck, R. Thouvenot, Vibrational investigations of polyoxometalates. 2. Evidence for anion-anion interactions in molybdenum(VI) and tungsten(VI) compounds related to the Keggin structure, Inorganic Chemistry, 22 (1983) 207-216.
[40] C. Rocchiccioli-Deltcheff, A. Aouissi, M.M. Bettahar, S. Launay, M. Fournier, Catalysis by 12-molybdophosphates: 1. Catalytic reactivity of 12-molybdophosphoric acid related to its thermal behavior investigated through IR, Raman, polarographic, and X-ray …, Journal of Catalysis, 164 (1996) 16-27.

[41] G. Ranga Rao, T. Rajkumar, B. Varghese, Synthesis and characterization of 1-butyl 3-methyl imidazolium phosphomolybdate molecular salt, Solid State Sciences, 11 (2009) 36-42.
[42] C.M. Granadeiro, P.M.C. Ferreira, D. Julião, L.A. Ribeiro, R. Valença, J.C. Ribeiro, I.S. Gonçalves, B. de Castro, M. Pillinger, L. Cunha-Silva, S.S. Balula, Efficient Oxidative Desulfurization Processes Using Polyoxomolybdate Based Catalysts, Energies, 11 (2018) 1696.
[43] D. Julião, A.C. Gomes, M. Pillinger, R. Valença, J.C. Ribeiro, I.S. Gonçalves, S.S. Balula, A recyclable ionic liquid-oxomolybdenum(vi) catalytic system for the oxidative desulfurization of model and real diesel fuel, Dalton Transactions, 45 (2016) 15242-15248.
[44] S. Fujita, M. Nishiura, M. Arai, Synthesis of styrene carbonate from carbon dioxide and styrene oxide with various zinc halide-based ionic liquids, Catalysis Letters, 135 (2010) 263-268.
[45] F. Mirante, L. Dias, M. Silva, S.O. Ribeiro, M.C. Corvo, B. de Castro, C.M. Granadeiro, S.S. Balula, Efficient heterogeneous polyoxometalate-hybrid catalysts for the oxidative desulfurization of fuels, Catalysis Communications, 104 (2018) 1-8.
[46] J. Xu, S. Zhao, W. Chen, M. Wang, Y.-F. Song, Highly Efficient Extraction and Oxidative Desulfurization System Using Na7H2LaW10O36·32 H2O in [bmim]BF4 at Room Temperature, Chemistry – A European Journal, 18 (2012) 4775-4781.
[47] W. Zhu, W. Huang, H. Li, M. Zhang, W. Jiang, G. Chen, C. Han, Polyoxometalate-based ionic liquids as catalysts for deep desulfurization of fuels, Fuel Processing Technology, 92 (2011) 1842-1848.
[48] S.O. Ribeiro, L.S. Nogueira, S. Gago, P.L. Almeida, M.C. Corvo, B.d. Castro, C.M. Granadeiro, S.S. Balula, Desulfurization process conciliating heterogeneous oxidation and liquid extraction: Organic solvent or centrifugation/water?, Applied Catalysis A: General, 542 (2017) 359-367.